The electrostatic force in blowing snow
by David Scott Schmidt

A thesis submitted in partial fulfillment of the requirements for the degree of Doctor of Philosophy in Civil Engineering
Montana State University

Abstract:
In blizzards and sand storms, wind transport of particles is associated with separation of electrostatic charge. Moving particles develop charge of sign opposite the electrostatic charge on stationary surface particles. This electrification produces forces, in addition to the gravitational and fluid friction forces, that determine trajectories for particles being transported in saltation. Evaluating electrostatic forces requires the electric field strength very near the saltation surface and charge-to-mass ratios for the moving particles.

Measurements in a blizzard provide an electric field profile, with measured fields as high as 30 kV m-1 measured at the 4-cm height. Reversal of charge sign on samples of saltation particles collected in a blizzard indicates a mixture of positive and negative particles in transport. This result points out the need for measurements of charge on individual particles, and an apparatus designed to make these measurements is detailed. Using measured charge-to-mass ratio for individual saltation particles (Schmidt et al., 1998) of +72 mC kg-1 and -208 mC kg'1 we estimate electrostatic forces as large as the gravitational force on some saltating particles. Including forces of this magnitude in the equations of motion for saltating particles shows saltation trajectories altered as much as 60% from those for uncharged particles.

These results show that the electrostatic force has a significant effect on the saltation process which brings up questions about the effects of the electrostatic force on the transfer of momentum from the atmospheric boundary layer to the planetary surface and wind transport of particles by suspension in the atmosphere.

THE ELECTROSTATIC FORCE IN BLOWING SNOW

by

David Scott Schmidt

A thesis submitted in partial fulfillment
of the requirements for the degree

of

Doctor of Philosophy

in

Civil Engineering

MONTANA STATE UNIVERSITY-BOZEMAN
Bozeman, Montana

January 1999

APPROVAL

of a thesis submitted by

David Scott Schmidt

This thesis has been read by each member of the thesis committee and has been found to be satisfactory regarding content, English usage, format, citations, bibliographic style, and consistency, and is ready for submission to the College of Graduate Studies.

Jimmie Dent — (Signature) — 13 Jan 99 — Date

Approved for the Department of Civil Engineering

Don Rabern — Donald G. Rabern — (Signature) — 1/13/99 — Date

Approved for the College of Graduate Studies

Bruce R. McLeod — Bruce R. McLeod — (Signature) — 1-14-99 — Date

STATEMENT OF PERMISSION TO USE

In presenting this thesis in partial fulfillment of the requirements for a doctoral degree at Montana State University-Bozeman, I agree that the Library shall make it available to borrowers under the rules of the Library. I further agree that copying of this thesis is allowable only for scholarly purposes, consistent with fair use as prescribed in the U.S. Copyright Law. Requests for extensive copying or reproduction of this thesis should be referred to University Microfilms International, 300 North Zeeb Road, Ann Arbor, Michigan 48106, to whom I have granted "the exclusive right to reproduce and distribute my dissertation in and from microform along with the non-exclusive right to reproduce and distribute my abstract in any format in whole or in part."

Signature Scotty Schmidt

Date 13 JAN 99

ACKNOWLEDGMENTS

The author would like to take this opportunity to thank Dr. Herald Kirkham and Shannon Jackson at the Jet Propulsion Laboratory for the generous loan of the DC electric field meter without which these measurements could not have been made.

My heartfelt thanks to Fay Johnson and the Bridger Bowl Ski Patrol. Without your friendship and financial support in the final months, the completion of this degree would not have been possible.

Thank you to Dr. Jimmie Dent for allowing me the freedom to do things my way even when I was wrong, and to Dr. Ed Adams for his support and participation in many of my endeavors that were right. Special thanks to Dr. Theodore Lang, not only for giving me the opportunity to learn and practice the fine art of teaching, but also for showing me what it means to teach well.

Most importantly, my sincerest thanks to Dr. R.A. Schmidt of the U.S. Forest Service, Rocky Mountain Forest and Range Experiment Station, for the generous loan of equipment without which these experiments would not have been possible. For all his help and guidance in designing and building the various apparatus used. For the countless hours spent together in Wyoming blizzards. But mostly, thank you for being the best friend and Father a fella' could have.

TABLE OF CONTENTS

TABLE OF CONTENTS Continued

LIST OF TABLES

LIST OF FIGURES

LIST OF FIGURES Continued

ABSTRACT

In blizzards and sand storms, wind transport of particles is associated with separation of electrostatic charge. Moving particles develop charge of sign opposite the electrostatic charge on stationary surface particles. This electrification produces forces, in addition to the gravitational and fluid friction forces, that determine trajectories for particles being transported in saltation. Evaluating electrostatic forces requires the electric field strength very near the saltation surface and charge-to-mass ratios for the moving particles.

Measurements in a blizzard provide an electric field profile, with measured fields as high as 30 kV m^{-1} measured at the 4-cm height. Reversal of charge sign on samples of saltation particles collected in a blizzard indicates a mixture of positive and negative particles in transport. This result points out the need for measurements of charge on individual particles, and an apparatus designed to make these measurements is detailed. Using measured charge-to-mass ratio for individual saltation particles (Schmidt et al., 1998) of +72 mC kg^{-1} and -208 mC kg^{-1} we estimate electrostatic forces as large as the gravitational force on some saltating particles. Including forces of this magnitude in the equations of motion for saltating particles shows saltation trajectories altered as much as 60% from those for uncharged particles.

These results show that the electrostatic force has a significant effect on the saltation process which brings up questions about the effects of the electrostatic force on the transfer of momentum from the atmospheric boundary layer to the planetary surface and wind transport of particles by suspension in the atmosphere.

CHAPTER ONE

INTRODUCTION

Wind is an incredibly powerful force capable of moving vast quantities of snow during blizzards. Deposition of wind-blown snow forms large drifts that hamper winter travel in many regions of the world. Billions of dollars are spent annually in an effort to keep roads and railways clear of drifting snow. In mountainous regions, cornices and wind-deposited snow in the lee of ridges trigger avalanches that damage structures and transport systems. Effective control of this natural phenomenon requires a better understanding of the physical processes that govern the transport of snow.

Wind transports snow by three mechanisms. Particles roll along the surface in a process termed creep. This mechanism occurs in light winds and accounts for very little transport. Strong winds eject particles from the surface in a mode of transport called saltation. Particles in saltation bounce along the surface, rebounding to heights typically within 10 cm of the surface. Most of the transport during blowing snow storms moves in saltation. In the third transport mode, known as suspension, particles travel without impact, at heights that may extend several hundred meters in polar storms. Saltating particles are the

source for suspended transport, therefore understanding saltation is essential to controlling blowing snow.

The Saltation Process In Blowing Snow

In describing the motion of sand particles in water, Gilbert (1914) used the word saltation, to describe the hopping motion of sand particles near the flow bed. Later, Bagnold (1941) showed that this same mechanism occurred in wind-blown sand, and Kobayashi (1972) first photographed saltation occurring in drifting snow.

Saltation of snow in air occurs when wind across a snow surface exceeds a threshold speed above which particles are dislodged and ejected into the flow. Once dislodged, the snow particles bounce along the boundary, within a few centimeters of the surface. Photographs show the particles are often rounded by abrasion, with equivalent spherical diameters ranging from 0.1 to 0.5 mm (Schmidt, 1981). Kobayashi (1972) estimated trajectory lengths as large as 1 m in moderate drifting, with mean lengths between 0.1 and 0.3 m for wind speeds of 10 m s^{-1} at 1 m height.

The restitution coefficient of an ice sphere bouncing on an ice block ranges from 0.6 to 0.9 as temperature decreases from -5 to -20 C, (Kobayashi, 1972). As a result, impacts of saltating snow are sufficient to fracture ice bonds holding surface grains (Schmidt, 1980) and impact energy may be transferred to several new particle trajectories. This rebounding of particles on the surface transfers significant momentum from the atmosphere to the planetary boundary

(Kikuchi, 1981), and results in a drag on the wind that is reflected in the vertical velocity profile (Maeno et al. 1979).

Whether it be snow or sand particles in air, sediment in a river bed, or sand in a density current on the ocean floor, the equations that describe saltation are of similar form. Particle rebound from elastic impact with surface particles to follow long, low trajectories in response to forces of fluid drag and gravitation. Using a high-speed camera to photograph trajectories of saltating glass spheres in a wind tunnel, White and Schultz (1977) found trajectories were higher and longer than predicted from equations involving only fluid drag and gravitational forces. They improved agreement with the observed trajectories by adding Magnus lift to the theoretical equations. However, matching measured trajectories by the addition of Magnus effect required large spin rates, in the range of 100 to 300 revolutions per second. Another force that could add or subtract lift is the electrostatic force that develops due to frictional rubbing between the particles and surface as they saltate.

A charged particle, moving in an electric field, is subject to an electrostatic force. The magnitude of the force is equal to the product of the electric field and the charge on the particle. The force acts along the electric field vector, in the direction determined by the sign of the particle charge. The purpose of the research presented in the following thesis was to measure the electrostatic force in blowing snow and analyze its effect on particle saltation trajectories. Equations of motion for a saltating sphere subject to an electrostatic force are developed. Measurements of the electric field during a blizzard as well as

particle charge are presented. Finally, the equations of motion are solved, using this experimental data, showing the effects of electrification on saltation.

CHAPTER TWO

ELECTRIFICATION OF BLOWING SNOW

The Electrostatic Force

Two charges q and Q, separated by a distance r, experience a Coulomb force defined by

$$\mathbf{F} = \frac{qQ}{4\pi\varepsilon r^2}\mathbf{r}. \tag{2.1}$$

Here, $4\pi\varepsilon$ is a proportionality constant, with ε being the free permittivity of space. This force acts over a distance and is therefore a field force associated with an electric field analogous to the gravitational force and field that results from the separation of mass. By definition the electric field is the force on Q per unit test charge q so that

$$\mathbf{E} \equiv (\frac{\mathbf{F}}{q}) = \frac{Q}{4\pi\varepsilon r^2}\mathbf{r} \tag{2.2}$$

Equation (2.2) is known as Coulomb's Law. Equations (2.1) and (2.2) allow us to state that the force on charge q due to the electric field **E** is

$$\mathbf{F} = q\mathbf{E}. \tag{2.3}$$

The electric potential Φ of a unit charge in an electric field is defined by the work necessary to move the charge from $r = \infty$ to $r = r_o$ against the electric field so that

$$\Phi = \int_{\infty}^{r_o} \frac{Q}{4\pi\varepsilon r^2}\mathbf{r}\cdot d\mathbf{r} \tag{2.4}$$

or, conversely,

$$\mathbf{E} = -\nabla\Phi . \tag{2.5}$$

For any vector field we can define a flux through a surface. For the electric field **E** the electric flux through some surface S is

$$f = \int \mathbf{E}\cdot d\mathbf{S} . \tag{2.6}$$

Using Coulomb's Law we can write

$$\mathbf{E}\cdot d\mathbf{S} = \frac{Q}{4\pi\varepsilon r^2}\mathbf{r}\cdot d\mathbf{S} . \tag{2.7}$$

The dot product $\mathbf{r}\cdot d\mathbf{S}$ is the projected area element on the surface of a sphere of radius r. In spherical coordinates this is given by

$$\mathbf{r}\cdot d\mathbf{S} = (rd\theta)(r\sin\theta d\phi) = r^2 d\Omega \tag{2.8}$$

where $d\Omega$ is often referred to as the differential solid angle. The integral of $d\Omega$ over a closed surface is 4π so that combining equations (2.7) and (2.8) gives

$$\oint \mathbf{E}\cdot d\mathbf{S} = \frac{Q}{\varepsilon} . \tag{2.9}$$

Equation (2.9) for a single point charge generalizes, by the superposition principle, to the net charge density $\rho(r)$ inside the surface

$$\oint \mathbf{E} \cdot d\mathbf{S} = \frac{\rho}{\varepsilon}. \tag{2.10}$$

Using the divergence theorem (2.10) can be rewritten as

$$\int (\nabla \cdot \mathbf{E}) dV = -\int (\nabla^2 \Phi) dV = \frac{\rho}{\varepsilon}. \tag{2.11}$$

Since the choice of volume is arbitrary this result must not depend on the volume integration but rather the integrand, implying

$$\nabla^2 \Phi = -\frac{\rho}{\varepsilon}, \tag{2.12}$$

which is Poisson's Equation.

Electric Fields In The Atmospheric Boundary Layer

Electric fields result from a separation of positive and negative charge. During periods of fair weather, ionization of air by gamma radiation, both terrestrial and from space, creates an electric field in the atmosphere that decreases with height above the Earth's surface. This fair-weather field varies considerably over time and location, with the average fair-weather field 1 m above the Earth's surface being -120 V m^{-1}. The negative field vector points toward the Earth's center, indicating positive charge located over negative charge in the atmosphere (Iribarne and Cho, 1980).

During dust storms and blizzards, the field increases in magnitude and reverses direction in the region occupied by blowing particles (Schonland, 1953). Many observers have reported electrification of natural blowing snow. Simpson (1921), Sheppard (1937), Schaefer (1947), Pierce and Currie (1949), Barre (1953), and Magono and Sakurai (1963) all observed a considerable increase in the positive electric field gradient normal to the earth's surface during blowing and drifting snow events. This would indicate negative charge positioned over a positively charged surface. Assuming that the electric field E is a function of height alone, the relationship between electric field and charge density ρ is given by Poisson's equation

$$\frac{dE}{dz} = -\frac{\rho}{\varepsilon}, \tag{2.13}$$

where z is height above the surface. The charge density decreases rapidly with height as transported particle density decreases so that the electric field diminishes with increasing height through the transportation region. At some point a balance between atmospheric charge and surface charge must exist at which point the electric field is zero. The total electric field at any height h is found by separating variables and integrating expression (2.13) so that

$$E_h = \frac{1}{\varepsilon_0} \int_0^h \rho dz. \tag{2.14}$$

so that the electric field is simply a function of the charge density between the surface and any given height h.

The field strength at which the insulating properties of air breaks down and allows electrical discharge provides an upper limit, near 3000 kV m^{-1} [Iribarne and Cho, 1980]. Results of such discharges depend on the amount of charge separation. Effects range from unobserved point discharges (most likely the case for blowing sand or snow on Earth) to the legendary Saint Elmo's fire at the pointed end of ships' masts during storms at sea, and the spectacular display of lightning following separation of enormous quantities of charge in thunderstorms.

Charge Separation In Ice

Efforts to explain electrification in thunderstorms produced most of the knowledge on charge separation mechanisms in ice. Several theories explaining thunderstorm electrification have developed since the early 1940's, but at this point, the process is not entirely understood. Lightning is the result of charge separation in clouds extending above heights at which the air temperature is 0°C. The main thunderstorm dipole develops in the region of the cloud where temperatures are well below freezing. This lead early researchers to conclude that the ice phase, or transition to the ice phase was responsible for thunderstorm electrification. Workman and Reynolds (1950) showed that large charge separation results as aqueous solutions freeze. They associated this charge separation (termed the Workman-Reynolds effect) to migration of contaminants along concentration gradients between the solid and liquid phase. Reynolds et al. (1957) hypothesized that impacts of ice crystals with a graupel

pellet would create a liquid film by pressure contact, producing charge separation during regelation.

Latham and Mason (1961) demonstrated that charge separation in ice resulted from temperature gradients. Hobbs (1974, p. 179) reviews the theory of this process, termed the thermoelectric effect. Concentrations of H^+ and OH^- ions increase as the temperature on an ice specimen increases. H^+ ions have greater mobility in the ice lattice than OH^- ions, therefore they migrate more rapidly along a concentration gradient. When a temperature gradient in the ice produces an ionic concentration gradient, H^+ ions move more rapidly to colder regions. The process develops a potential difference across uniform pure ice of (2.3±0.3) mV for each degree C of temperature difference (Hobbs, 1974).

Latham and Mason (1961) extended this theory to two separate ice specimens. When two pieces of ice, at different temperatures, were brought into contact for a short period of time (10^{-3} s) and then separated, the warmer piece of ice acquired a negative charge while the cooler piece became positively charged.

Tabor (1951) estimates a contact time between colliding particles on the order of 10^{-7} s. Gross (1982) shows that, theoretically, substantial charge can be transferred in this time span for pure ice-ice collisions and that transfer is enhanced with the introduction of impurities.

Electrification In Blizzards

From laboratory experiments on the electrification of wind-blown snow, Latham and Stow (1967) suggested three processes for charge separation, all involving the thermoelectric effect. In their discussion, the processes are: (1) crystal fragmentation, (2) asymmetric rubbing, and (3) transient contact of blown particles with the surface. Each is described below. They found contributions to electrification by the Workman-Reynolds effect, and by evaporation of ice, were minimal.

Process (1), crystal fragmentation, separates charge when a temperature gradient exists across the crystal. Such a gradient might exist when the temperature of the wind differs from the snow temperature below the surface. If the wind is warmer, the most exposed projections on the surface are warmed, and become negatively charged. If such a fragment breaks from the surface, it carries a net negative charge.

Asymmetric rubbing, process (2), refers to a difference in contact areas when two ice pieces rub together. If a small ice crystal slides along a larger ice surface, the contact area of the crystal remains small, while the area contacted on the surface increases with time. Greater frictional heating of the crystal results, and the warmer crystal gains a negative charge. Henry (1953) described charging of insulators by asymmetric rubbing, which was demonstrated with ice by Reynolds et al. (1957), and Latham (1963).

By process (3), if a temperature gradient exists over the areas of contact, charge will be transferred during the transient contact of a blown particle with the surface. If air flow is warmer than the surface, particles receive negative charge during contact, since surface particles have negatively charged extremities, as in process (1). Net charge on the surface becomes opposite in sign. The signs are reversed if colder air creates saltation across a warmer surface.

Latham and Stow (1967) based their conclusions upon measurements of charging as a function of particle concentration, wind speed, temperature difference between the air and snow surface, and relative humidity. In their experiment they found charging of wind blown particles to be a strong function of wind speed, with charge increasing approximately as wind speed squared. The temperature difference ΔT between the air jet used to transport saltation particles and the snow surface had a significant effect on particle charge, particularly charge sign. Here, ΔT is positive when air temperature is greater then surface temperature. Their results indicate that particle charging is a minimum when ΔT is zero. Saltating particles became more negatively charged when ΔT was positive. Saltation particle concentrations play a role in particle charging as a function of ΔT. During low level transport of 1 g s^{-1} the net charge measured on the blowing particles switched from positive to negative, opposite the change in sign of ΔT. When mass flux was increased to 10 g s^{-1} the net charge on the saltation particles remained negative for all ΔT, with the magnitude of the charge increasing as ΔT went from negative to positive. Measurements of the effects of

relative humidity on particle charging were confounded by instrumentation problems in Latham and Stow's (1967) experiment. They were able to show, however, that electrification increased as relative humidity decreased. In wind tunnel experiments, Maeno et al. (1985) also measured electrification as a function of temperature and wind speed. They found charging of blowing particles increased as wind speed increased and air temperature decreased. Their measurements did not include differences in air and surface temperatures.

A fourth process Latham and Stow (1967) suggested, ionization of air by point discharge as highly charged particles rebound from the surface, depends on the amount of charge separation developed by the first three. Their hypothesis was based on measurements (Latham and Miller, 1965) showing increasing production of ions by point discharge as wind velocity increases. As Hobbs (1974) pointed out, the relative importance of these processes under natural conditions remained to be determined. Apparently this is still the case.

Other theories explain charge separation in thunderstorms without the thermoelectric effect. Scott and Levin (1970) describe polarization of ice particles by a potential gradient, which enhances charge separation during collisions with smaller ice crystals. The force associated with collision between particles, and roughness of the ice surfaces are also factors. Scott and Hobbs (1968) show that the sign of the charge acquired by an ice specimen from a collision depends on the shapes of the particles involved and that magnitudes of the acquired charge increases with increased impact velocities. Latham and Stow (1965) found that charge transfer associated with the thermoelectric effect

could be greatly enhanced if the ice specimens are rough and if impact velocities are high. They attribute their results to the delicate nature of rough particle appendages and increased particle fragmentation with increasing impact forces.

In general, the results of Latham and Stow's (1967) experiments support the hypotheses of the thermoelectric effect as the charging mechanism for windblown particles, but also suggests a complicated relationship between the charge that develops on the particle and the environment the particle travels in.

Equations for Saltation in an Electrostatic Field

In this section, we add electrostatic forces from equation (2.3) to the equations for saltating motion developed by White (1975), as presented in White and Shultz (1977). Forces acting on the moving particle include lift forces, fluid drag forces, and gravitational force $m_p\mathbf{g}$, where m_p is the mass of the particle and $\mathbf{g}$ is gravitational acceleration. The additional electrostatic force is $q\mathbf{E}$, where q denotes particle charge, and $\mathbf{E}$ is the electric field. Following notation in White and Shultz (1977), the horizontal, vertical, and rotational components of motion for a charged particle saltating in an electric field are

$$m_p \ddot{x} = L\left(\frac{\dot{y}}{V_r}\right) - D\left(\frac{\dot{x}-u}{V_r}\right) + E_x q, \tag{2.15}$$

$$m_p \ddot{y} = -L\left(\frac{\dot{x}-u}{V_r}\right) - D\left(\frac{\dot{y}}{V_r}\right) - m_p g + E_y q, \tag{2.16}$$

$$I_p \ddot{\theta} = M. \tag{2.17}$$

Here u is the velocity of the fluid (assumed to be traveling in the horizontal direction) which is a function of height y above the surface. I_p is the particle's moment of inertia, and $\ddot{\theta}$ is the particle's angular acceleration. E_x and E_y are the horizontal and vertical components of the electric field, and V_r is the velocity of the particle relative to the fluid flow. Its magnitude is

$$V_r = [(\dot{x}-u)^2 + (\dot{y})^2]^{1/2}. \tag{2.18}$$

Drag force D resulting from this relative velocity opposes motion of the particle and is expressed in terms of the drag coefficient C_d, as

$$D = \frac{1}{2} C_d A_p \rho V_r^2, \tag{2.19}$$

where A_p is the cross-section area of the particle, and ρ is the density of the fluid.

In the atmospheric boundary layer, the strong velocity gradient near the surface produces a pressure difference between the top and bottom of the particle, resulting in a lift force. This velocity gradient also produces a moment, causing the particle to spin, adding additional lift by Magnus effect. Total lift force on the particle is

$$L = \frac{1}{8}\pi d^3 \rho V_r (\dot{\theta} - \frac{1}{2}\frac{\partial u}{\partial y}), \tag{2.20}$$

where the lift force is coupled to the moment of the particle through the angular velocity $\dot{\theta}$ (defined as positive for clock-wise rotations) and d is particle diameter. The moment is

$$M = \pi\mu d^3(\dot{\theta} - \frac{1}{2}\frac{\partial u}{\partial y}), \tag{2.21}$$

with μ denoting fluid viscosity. We note that these equations describe the saltation trajectory for a sphere and are only an approximation to the trajectories of saltating sand and snow particles. The electrostatic charge is assumed to be uniformly distributed over the particle surface.

Electrostatic Force on Saltating Particles

Solving the equation for a charged saltation particle requires measurements of the particle charge and the electric field in the saltation region (typically 0 - 10 cm above the saltation surface). At the onset of this project measurements of average particle charge-to-mass ratios were available, however measurements of the electric field close to the saltation surface were lacking.

Several researchers have measured particle charge. Latham and Montagne (1970) measured average charge-to-mass ratios of -10 $\mu C\ kg^{-1}$ for snow blowing across a cornice. Wishart (1970) measured average charge-to-mass ratios as high as -50 $\mu C\ kg^{-1}$ in Antarctic drifting. Maeno et al (1985)

showed that negative charge also develops on snow particles saltating in a wind tunnel. The charge on surface particles varied from -0.01 $\mu C\ kg^{-1}$ to +0.03 $\mu C\ kg^{-1}$. These magnitudes were near those of the saltating particles, and sign changes appeared to coincide with local deposition and erosion areas on the surface. These researchers attributed lower charge-to-mass ratios, compared to those seen in natural blowing snow by Latham and Montagne (1970) and Wishart (1970), to the short fetch distance of their wind tunnel.

As will be shown, measurements made by Schmidt and Schmidt (1992) indicate average particle charge-to-mass ratios significantly underestimate actual particle charge. Nevertheless, these average values could be used as an estimate of particle charge. Solution of the saltation equations was still confounded by lack of electric field measurements. Latham and Montagne (1970) measured the field in the region 30-100 cm above the surface and found it varied significantly with height. In an effort to evaluate the effects of electrification on saltation, Schmidt and Dent (1993) proposed a theoretical model based on Latham and Montagne's (1970) data at distances far from the surface and the electric field due to a bed of charged ice spheres for the near-surface field.

Based on measurements of surface particle charge made in a wind tunnel (Maeno et al.,1985), the ice spheres were assumed to have a charge-to-mass ratio equal but opposite to that measured for blowing snow particles. The electric field above a bed of ice spheres, made up from rings of spheres arranged in closest packing, was computed as a function of height above the bed by treating

each sphere as a point charge and applying Coulomb's Law. Contributions to the field decreases rapidly as the radius of these rings increases, so that little was contributed beyond 10 rings, or the area covered by 61 bed spheres. This model allowed us to solve the saltation equations (2.15) - (2.21) using standard numerical techniques. The results predicted substantial changes in saltation trajectory lengths for charged particles compared to uncharged particles. These changes in trajectory lengths were consistent with observed trajectories.

Experimental evidence was obviously needed to verify the extent to which saltation is affected by electrification. Based on measurements made by Schmidt and Schmidt (1992), we questioned the validity of particle charge-to-mass ratios determined by measuring the average charge on a sample of blowing snow. Measurements of the electric field profile in the saltation region and the charge on individual particles became the focus of the research presented here. The remainder of this thesis details Schmidt and Schmidt's (1992) experiment. Measurements of the electric field profile in the saltation region are presented as well as measurements of the charge on individual blowing snow particles. Inclusion of this data in the saltation equations presented in the previous section leads to an analysis of the effects of the electrostatic force on the saltation process.

CHAPTER THREE

MEASUREMENTS OF THE ELECTRIC FIELD GRADIENT IN A BLIZZARD

Determining of the electric field profile in a blowing snowstorm requires a measuring device that can be placed close to the snow surface without affecting the measurements. In the past it was not possible to measure closer then 30 cm to the surface without disrupting the field (hence Latham and Montagne's 1970 measurements). Recent technologic advancements have resulted in electric field meters capable of making the needed near-field measurements. The meter used in this experiment was developed by the Jet Propulsion Laboratory (JPL) at the California Institute of Technology. The DC electric field probe is described in detail by Kirkam and Johnston (1989). The following is a description of the physics involved in its operation.

DC Electric Field Mill

The sensor is a cylindrical Fiberglass shell 25 mm in diameter and 33 mm long, rotating around the long axis. The cylinder is divided length-wise into two semi-cylinders of conductive paint, coating the outer surface of the shell, separated by a thin dielectric (Figure 1). The electric field induces a charge on the surface of the cylinder (figure 1). This induced charge is proportional to the

field. An air turbine (from a dentist drill) rotates the probe using compressed nitrogen in place of air as the driving agent. As the cylinder rotates, the charge on the surface remains fixed with respect to the electric field, inducing an alternating current between two electrodes mounted 180 degrees from each other on the cylinder's surface. A hybrid microcircuit inside the shell amplifies the oscillating signal and converts it to an optical pulse train by means of a light emitting diode. The pulse train is transmitted by optical fiber to a receiver that demodulates and resolves the signal into horizontal and vertical components of the measured electric field. The sensor is electrically isolated from the receiver and supported by a 1-m long Fiberglass wand clamped to the vertical support tube of an adjustable camera tripod. A calibrated ten-turn potentiometer mounted on the tripod produces voltages proportional to the height of the probe above the snow surface. Output from the receiver was recorded using a Campbell Scientific data logger (Model CR21). Moving the probe to various heights and sampling at 1 min intervals for periods of 15 min gave an average vertical profile of electric field strength. We confirmed probe calibration

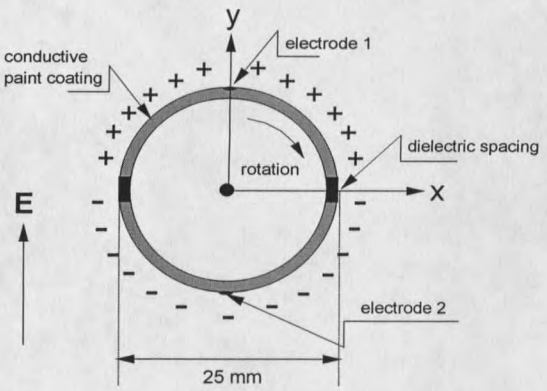

Figure 1: End view of electric field probe in an electric field. Charge is induced on simi-circular shells separated by a dielectric spacing. Rotation of the cylinder in the electric field results in the generation of a current between electrodes.

immediately after the measurements by centering it between two parallel, 50 cm square aluminum plates at 20 kV difference in potential.

Harold Kirkam made a generous loan of the DC electric field meter to Montana State University for the winter of 1993-94 in order that its operation be tested in harsh blizzard environments. The probe worked exceptionally well in winter conditions and in January 1994 measurements were made of the electric field in the region .002-4 m above the snow surface during blizzard conditions.

The Experiment

On 6 January 1994, a mobile laboratory was moved to a location just south of the Cooper Cove interchange of Interstate Highway 80, 50 km west of Laramie, Wyoming, at 41 31' N, 106 05'W, 2360m elevation. Consistent west winds during drifting over nearly level terrain with short-grass vegetation make the site nearly ideal for such measurements. These conditions exist for approximately 1 km upwind of the measuring location, beyond which terrain becomes more rolling for about 3 km to the foot of the Medicine Bow Mountains. 10 cm of new snow provided light drifting due to moderate winds. At 2458 hours on 7 January the wind increased from around 4 m s^{-1} to 10 m s^{-1} and up.

Instruments

An anemometer with 19 cm diameter, 3-cup plastic rotors produced signals with frequency proportional to wind speed. A thermistor shielded with a plastic pipe 'T' connector produced voltages proportional to air temperatures.

Both the average wind speed and temperature measurements were made at a 1 m height. Relative humidity at 2 m height was sensed in an enclosure mounted on the side of the mobile lab, and screened with polyester filter fabric. The electric field probe was connected to the receiver unit, housed in the mobile lab, by 15m fiber-optic cables.

Procedure

Computers in the mobile lab accumulated data from runs of 1 hour duration for storage on magnetic disks. Measurements of average wind speed, temperature, and humidity, as well as probe height and horizontal and vertical electric field components were recorded every minute. The procedure was simply to set the probe at a given height for a period of 15 min. Each time the probe height was changed a manual measurement was taken and compared to the height reading given by the potentiometer to insure accuracy. A series of vertical profiles for electric field above the snow surface was measured in the period 0100 h to 0630 h.

Results

Measurements of electric field were averaged at each height interval. The measured electric field as a function of height is shown in figure 2. We fit a power-law profile to the data in order to facilitate evaluation of saltation trajectories. The theoretic model of the electric field immediately above a bed of

charged spheres (Schmidt and Dent, 1993) was the basis for choosing the power-law fit.

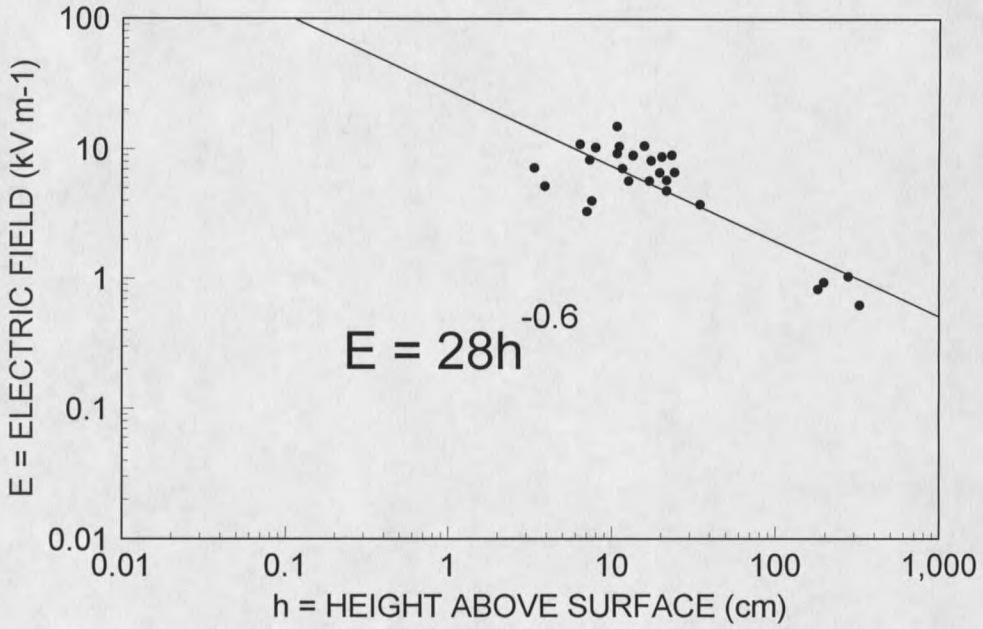

Figure 2: Electric field profile measured in blowing snow 7 Jan 94 using a DC electric field mill. Windspeed at the 1-m height averaged 12 m/s over the two hour measurement period. A power law fit to the data was used as an approximation for computational purposes based on a theoretical profile proposed by Schmidt and Dent (1993).

Discussion

The electric fields measured in this experiment were as much as 30 kV m^{-1} at a height of 4 cm as compared to the fair weather electric field of 0.06 kV m^{-1} measured at the same height. Electric fields measured in a blowing snow storm

compare surprisingly well with the theoretic model developed by Schmidt and Dent (1993).

As expected by a review of the charging mechanisms for ice particles (Hobbs, 1974) the electric field measured here appears to be a strong function of blowing snow particle flux. Based on the results of Lathem and Stow (1967) temperature and humidity must also play a role in the charging of the blowing snow particles. For the measurements made here temperature and humidity remained constant.

CHAPTER FOUR

THE SIGN OF ELECTROSTATIC CHARGE ON BLOWING SNOW

Based on a review of the mechanics by which charge separation develops in drifting snow, it seems likely that during stronger wind gusts, eroded surface particles with positive charge mix with negatively charged saltating particles. If, at some point, eroded particles dominate the mixture, this should lead to a reversal in the sign of charging current generated by accumulating drift particles in a suitable measuring trap. This chapter describes an experiment to detect such reversals and shows that the average sign of the charge on drifting snow particles can indeed change from negative to positive during periods of strong wind gusts. This new evidence strongly supports past findings indicating that blowing snow particles acquire negative charges while surface particles become positively charged. These results raise questions about the validity of average particle charge-to-mass ratios determined by measuring the total charge on a sample of blowing snow and dividing by the sample mass.

The Experiment

Measurements in a blizzard in southeastern Wyoming, on 9 and 10 January 1988, provide data for an initial test of the hypothesis. The location is

just south of the Cooper Cove interchange of Interstate Highway 80, 50 km west of Laramie, Wyoming, at 41 31' N, 106 05'W, 2360m elevation. This is the same location used by Schmidt and Dent (1994) in their experiment conducted 7 January 1994, reported in the previous chapter.

On 5 January 1988, a mobile laboratory was moved to the site. Electric power is available from a stub line that approaches from the northwest. Light snowfall with light north winds, during the evening of 5 January and all day on the 6th, added 10-15 cm of snow to old, hard snow dunes and drift features formed from a 60-cm snowfall, approximately 10 days earlier. Wind speed increased and drifting began about 1200 h on 7 January. Light snowfall and drifting continued throughout 8 January, during preparations for the electrostatic measurements. Interstate 80 was closed from Laramie west to Walcott Junction at 0950 h on 9 January, because of blowing and drifting snow. Measurements from two periods, 2100 h on the 9th to 0020 h on the 10th, and 0800 h to 1030 h on the 10th, are used in this thesis.

Instruments

Measurements included vertical profiles of average wind speed and temperature from 10 levels on a 10 m mast. A 2 m high pipe mast supported a wind vane and fast-response sensors of drift particle frequency, wind speed, and electric current generated by accumulating drift particles. An electronic barometer measured atmospheric pressure in the mobile laboratory. Relative

humidity at 2 m height was sensed in an enclosure mounted on the side of the mobile lab, and screened with polyester filter fabric.

Anemometers with 19 cm diameter, 3-cup plastic rotors produced signals with frequency proportional to wind speed, for the 10 m profile. Two-thermistor networks shielded with plastic pipe 'T' connectors produced voltages proportional to air temperatures at each level on that tower. Tabler (1980) gives details of the vertical profiling system.

A heated-thermistor anemometer (Kurz Mdl 1440M-4) provided a fast-response voltage proportional to wind speed near 18 cm above the surface at the 2 m mast. Although this sensor iced over in heavy drifting during the last runs on 9 January, readings for most of the experiment compared well with averages from the wind profile.

To sense drift rate, a photoelectric device called a snow particle counter (SPC) generated pulses from shadows of drift particles breaking a light beam. The sensing window is approximately 25 mm long and 3 mm high, normal to the wind. Height of this sensor above the snow surface was near 18 cm throughout the experiment. Electronics in the mobile lab produced a voltage proportional to a 5 s running average of the frequency of these pulses. Schmidt (1977) details this system.

The device constructed to measure the charging current produced by drifting snow particles is a portable Faraday Cage (Figure 3), similar in principle to the design reported by Wishart and Radok (1967). Two cylinders of brass screen are held concentric by insulating plastic. Polyester filter fabric (50-micron

mesh) covers each cylinder. Particles arrive at the inner cylinder through a copper tube insulated from the outer stainless steel support tube by plastic. Lifting the plastic swivel from its socket in the support arm and disconnecting the outer cylinder at the threaded coupling allows weighing of the trap and accumulated snow. A ball-bearing in the support swivel aids the fin in orienting the trap into the wind.

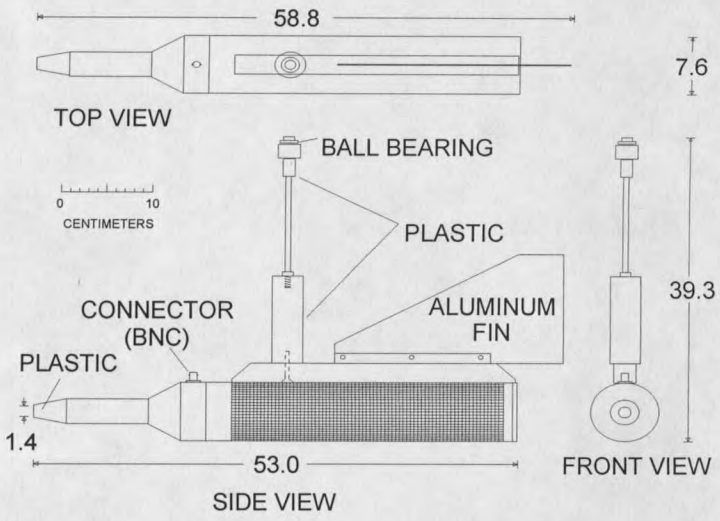

Figure 3: Diagram showing the dimensions of the portable Faraday cage. All dimensions are in cm.

The outer cylinder is electrically grounded by the shield of a 50 ohm coaxial cable with center conductor connected to the inner cylinder. The cable connects to an electrometer (Keithley Mdl 617) that measures the current conducted through a high resistance shunt between the two cylinders. The system ground was a copper rod driven in the ground at the rear of the mobile lab, approximately 4 m from the ground at the electric power pole.

Procedure

Computers in the mobile lab accumulated data from runs of 5 min duration for storage on magnetic disks. Wind profiles were plotted between runs. The system multimeter (Hewlett Packard Mdl 3455A) sampled signal voltages routed

by a multiplexer. Fast response data was sampled every 0.75 s, yielding 397 readings each for wind speed, drift frequency, and charging current during a 5 min run.

To test the portable Faraday Cage, the trap was plugged during some runs, and during two runs it was disconnected, to measure signal noise generated by the cable. Weighing snow in the trap on an electronic balance (Mettler Mdl PK36) after periods of several runs provided estimates of drift flux. During the night of 9 January, the trap sampled drift at 2-3 cm height. On the 10th, sampling was at 16 cm. Shining a spotlight windward at night permitted new snowfall to be detected as bright crystals amid the duller, rounded drift particles.

Results

Least-squares fits of the logarithmic wind profile equation (e.g., Schmidt, 1982) provided estimates of profile parameters $u*$, the friction velocity, and z_0, the roughness parameter. Table 1 lists these parameters for each run, together with temperature, humidity, and averages for the fast-response wind speed, drift rate, and charging current. Plotting reveals several pertinent changes in conditions (Figure 4). At approximately 2240 h, wind direction became more westerly by 25-30 degrees, relative humidity increased about 10%, and wind speed increased, with a corresponding increase in drift particle frequency.

New precipitation was observed in the spotlight beam starting at 2200h. It is likely that light snowfall occurred with the drifting during runs on 9 January, and unlikely during the period on 10 January. Figure 4 also indicates the status of the Faraday Cage (open, closed, or disconnected) during the experiment. By historical convention, the sign of electric current is defined as positive in the direction toward lower voltage potential. Negative current through the electrometer corresponds to a negative potential on the inner cylinder of the trap, with respect to the outer cylinder (system ground). Actual flow of electrons is from negative potential to ground.

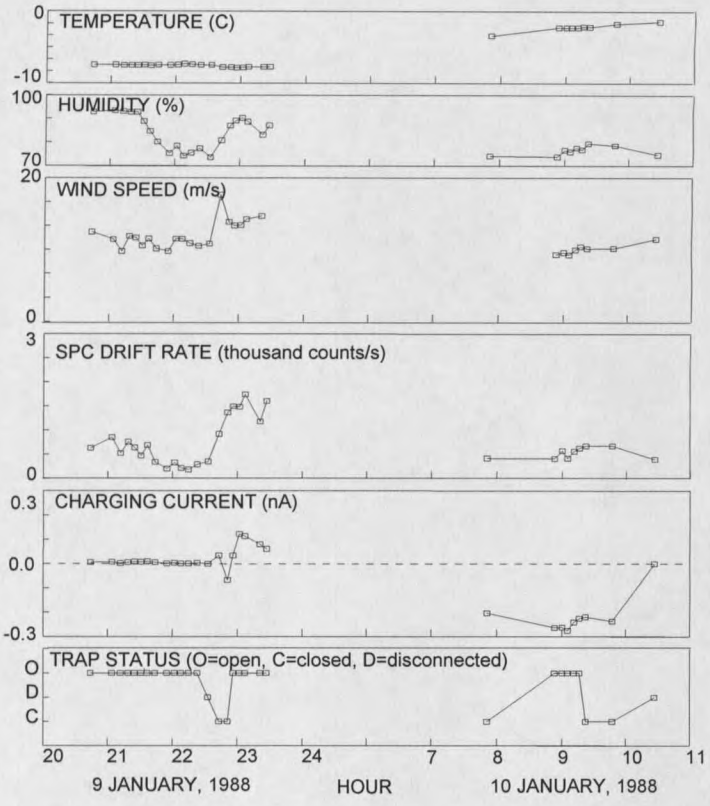

Figure 4: Average values during 5 min. runs show changes for the two data collection periods during the 9-10 January, 1988 blizzard.

Table 1. Average Conditions During 5-min Runs On 9-10 January 1988.

RUN NO	TIME (hhmm)	WIND AZ (deg)	u* (cm/s)	z_0 (cm)	RH (%)	TEMP (C)	DRIFT (no/s)	CURRENT (Na)	WIND (cm/s)
10902	2021	302	46.9	0.064	84	No disk file, program error			
10903	2044	305	55.4	0.108	93	-7.4	628	0.006	1244
10904	2104	301	59.0	0.085	93	-7.4	851	0.007	1144
10905	2112	300	56.1	0.061	93	-7.5	525	0.003	977
10906	2119	299	63.0	0.080	93	-7.5	757	0.006	1185
10907	2125	302	60.1	0.064	93	-7.5	638	0.009	1165
10908	2131	301	59.3	0.087	89	-7.5	473	0.007	1054
10909	2137	301	60.2	0.075	85	-7.5	690	0.010	1150
10910	2144	301	53.2	0.057	80	-7.5	339	0.006	1013
10911	2155	308	51.8	0.054	75	-7.5	205	0.002	977
10912	2202	308	60.0	0.057	78	-7.4	325	0.004	1149
10913	2208	308	60.4	0.058	74	-7.3	217	0.001	1148
10914	2215	310	57.9	0.061	76	-7.4	186	0.001	1089
10915	2223	311	56.3	0.057	77	-7.4	291	0.004	1049
10916	2233	301	58.5	0.088	74	-7.5	350	0.000	1081
10917	2243	291	69.8	0.111	81	-7.8	921	0.035	1762
10918	2251	282	81.7	0.137	87	-7.8	1365	-0.067	1383
10919	2256	280	77.7	0.130	89	-7.8	1494	0.035	1331
10920	2302	280	81.6	0.124	90	-7.8	1485	0.123	1338
10921	2307	280	91.0	0.174	89	-7.7	1743	0.114	1421
10922	2321	284	75.4	0.114	83	-7.7	1181	0.081	1467
10923	2327	283	86.1	0.129	87	-7.7	1606	0.061	2510
10924	2332	280	79.1	0.110	88	--------Disk Full Error-----			
----------Observers sleeping (sic)----------									
11003	751	285	82.0	0.195	74	-3.4	419	-0.204	205
11004	853	282	82.8	0.236	74	-2.2	410	-0.263	930
11005	900	279	83.1	0.158	77	-2.2	574	-0.262	958
11006	905	283	85.1	0.236	76	-2.2	416	-0.275	927
11007	911	281	83.8	0.169	78	-2.2	563	-0.241	997
11008	916	281	87.7	0.181	77	-2.1	626	-0.226	1038
11009	922	278	84.5	0.171	80	-2.1	674	-0.219	1012
11010	947	282	83.1	0.185	79	-1.7	674	-0.237	1016
11011	1027	279	87.9	0.383	75	-1.4	398	-0.001	1145

The plot of average drift charging current (Figure 4) shows a small, positive current during the light drifting through 2223 h on 9 Jan, indicating a net positive charge on the drift particles. The trap was disconnected for weighing at 2233 h, and connected but closed (intentionally plugged) between 2243 -2251 h. Stronger positive current was recorded with the trap open between runs 2256 - 2327 h. In contrast, the sign of the charging current was negative, and consistently stronger during drifting on the 10th, reflecting net negative charge on the incoming particles. The drift trap was open between 0853 - 0916 h.

Measured current during runs when the trap was opened or closed part way through the run show current fluctuations as large, but more frequent and

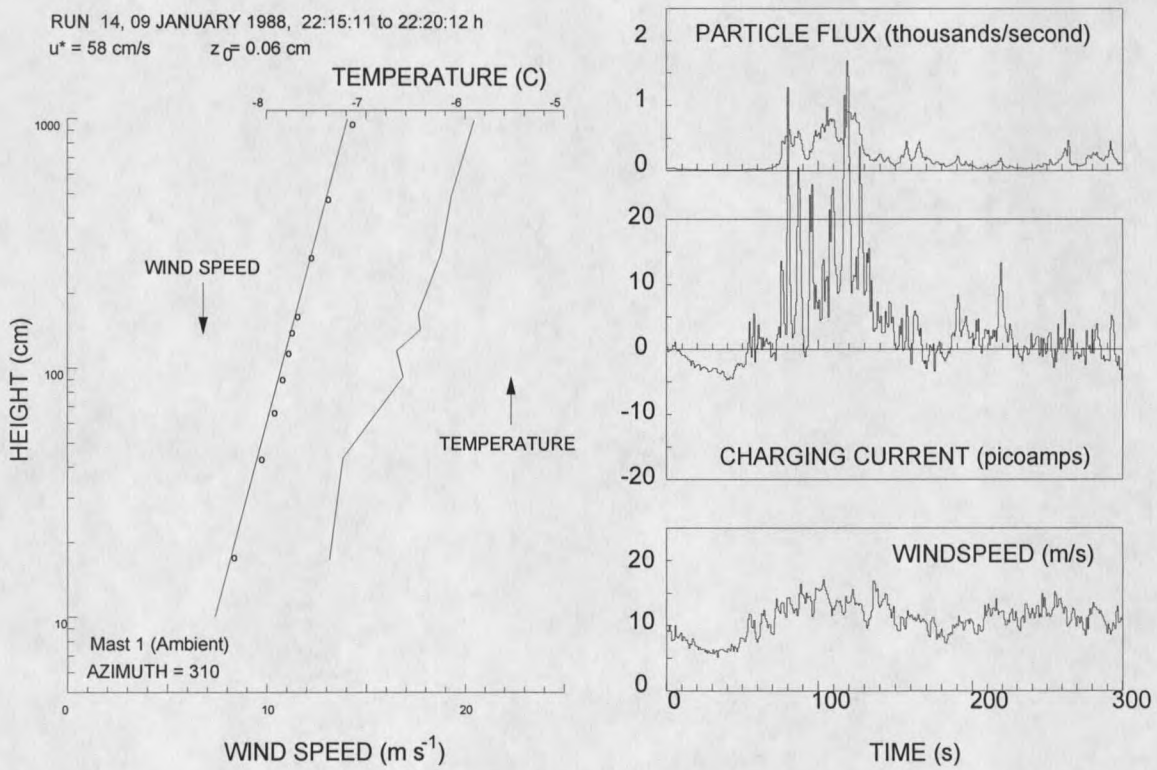

Figure 5: An example plot of data for run 10914, showing the 5-min average vertical profile for wind speed and temperature on the left, and fast-response particle frequency, wind speed, and charging current on the right.

less correlated with drift rate, when the trap was closed. The average current shifted in the sign direction of other runs within the period, when the trap was opened.

Figure 5 is an example plot of both vertical profile and fast response data, for run 14 on 9 January. All vertical temperature profiles showed about 1°C colder air at 18 cm than at 10 m, indicating a slightly stable stratification. This was true of both data periods, even though temperatures were higher during runs on the 10th. Comparison plots of particle flux and charging current (figure 5) shows a strong correlation between positive charging associated with increased drifting due to wind gusts.

Discussion

The experiment clearly shows extended periods of positive and negative charge on the inner cylinder of the portable Faraday Cage (Figure 4). Charge reversal corresponding to wind gusts and bursts of drift particles are also evident (Figures 5). However, several shortcomings of this experiment make a test of the hypothesis less than satisfactory. The difference in temperature, and difference in sample height of the Faraday Cage, between runs on the 9th, with positive current, and runs with negative current on the 10th, confound the test. Lack of data during the 8 h between the periods also frustrates us, since there is no way to know if the change in sign was gradual or rapid. Occurrence of snowfall during the first period added complication. Finally, the noise generated

by the cage when closed makes one question whether a test is even possible with this apparatus.

The hypothesis is significant in interpreting charge-to-mass ratios previously reported for drifting snow. If such measurements are derived by weighing samples of particles with a mixture of sign, they underestimate the ratios for individual particles. The force that a saltating snow particle experiences depends on the particle's charge-to-mass ratio and the electric field it travels in. The model electric field presented by Schmidt and Dent (1993), based on previously measured charge-to-mass ratios, indicates the electrostatic force on blowing snow particles may change saltation trajectories substantially. If particle charge-to-mass ratios are larger then those previously reported, the force on blowing snow particles would be even larger then predicted by the proposed model.

CHAPTER FIVE

MEASUREMENTS OF THE CHARGE-TO-MASS RATIOS ON INDIVIDUAL BLOWING SNOW PARTICLES

Based on the results of Schmidt and Schmidt (1992) we still questioned the magnitude of the particle charge-to-mass ratios on individual saltation particles. The following chapter details an experiment designed to measure the charge on individual blowing snow particles.

In his famous experiment, Millikan (1910) measured the charge of single electrons from the motion of oil drops moving in a constant electric field. Camp (1977) used a variation on this technique to determine charge-to-mass ratios for falling snow crystals. Based on their methods we designed the apparatus and experiment described below to measure the charge on drifting particles.

Equations Of Motion

A charged particle moving through still air, with a horizontal electric field, is acted upon by the gravitational force mg, an electrostatic force F_E, and a drag force F_d, due to air resistance, that opposes the particle's motion. If the direction the particle travels is defined by an angle θ with the vertical (Figure 6), the equations that describe the particle's motion are

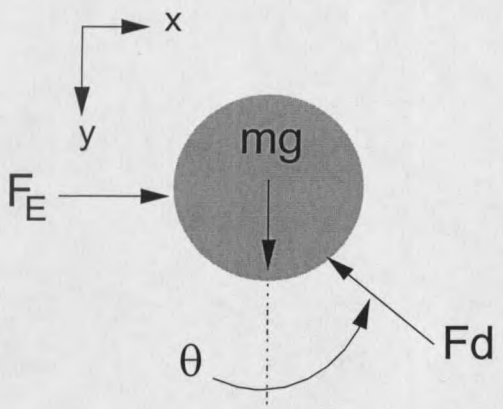

Figure 6: Free-body diagram of particle falling in air, subject to a constant electrostatic force.

$$F_E - F_d \sin\theta = m\ddot{x} \qquad (5.1)$$

and

$$mg - F_d \cos\theta = m\ddot{y} \qquad 5.2)$$

The magnitude of the electrostatic force is $F_E = qE$, where E is the magnitude of the electric field and q is the charge on the particle. For non-spherical particles traveling at low speed, the magnitude of the drag force can be approximated as $F_d = k(3\pi\mu)d_n v$ (McNown, et. al., 1951). Here k denotes the shape factor of the particle, μ is the dynamic viscosity of air, d_n is the particle's nominal diameter, and v is the velocity of the particle. Note the difference between F_d and the drag force D defined by equation (2.19). Settling velocities for small particles are associated with low Reynolds numbers Re less then 10. For Reynolds numbers in this range the drag coefficient term in equation (2.19) can be approximated by Stokes Law

$$C_d = \frac{24}{Re}.$$

Substituting this expression for the drag coefficient C_d in equation (2.19) and simplifying based on the dimensions of a sphere gives

$$D = 3\pi\mu d_n v.$$

McNown et al. (1951) shows that this expression is not in good agreement with the drag on particles moving at the slow speeds associated with settling. They

attribute this observation to the increased effects of particle shape on drag as speeds decrease so that the shape factor k must be included in the drag force F_d. Substituting F_d into equations (5.1) and (5.2) gives

$$qE - k_x(3\pi\mu)d_n v\sin\theta = m\ddot{x} \tag{5.3}$$

and

$$mg - k_y(3\pi\mu)d_n v\cos\theta = m\ddot{y} \tag{5.4}$$

$(v)\sin\theta$ and $(v)\cos\theta$ are the horizontal and vertical components of particle velocity so that

$$qE - k_x(3\pi\mu)d_n \dot{x} = m\ddot{x} \tag{5.5}$$

and

$$mg - k_y(3\pi\mu)d_n \dot{y} = m\ddot{y} \tag{5.6}$$

Assuming the particle falls at terminal velocity v_T, the vertical component of acceleration is zero, and the vertical component of velocity is constant. Equation (5.6) then becomes $mg = k_y(3\pi\mu)d_n v_T$ which can be rearranged as

$$\frac{k_y}{m} = \frac{g}{(3\pi\mu)d_n v_T} \tag{5.7}$$

If the particle rotates as it falls, the particle will have a random orientation with time. If we average k over time, the shape factor will be the same for all directions so that $k_x = k_y$. Dividing equation (5.5) by particle mass and substituting equation (5.7) for k_x/m gives

$$E(\frac{q}{m}) - (\frac{g}{v_T})\dot{x} = \frac{d\dot{x}}{dt} \qquad (5.8)$$

Equation (5.8) expresses the motion of the particle in terms of the variables E and v_T (which can be measured experimentally) and the ratio q/m which we wish to determine. Equation (5.8) is solved by separation of variables. For brevity, we define the two constant expressions in equation (5.8) as E(q/m) = a and (g/v_T) = b. Substituting these expressions into equation (5.8), separating variables, and integrating both sides of the resulting expression gives

$$\int \frac{d\dot{x}}{a - b\dot{x}} = \int dt$$

or

$$t = -\frac{1}{b}\ln[a - b\dot{x}] + c_1 \qquad (5.9)$$

We evaluate the constant of integration c_1 by assuming the x - component of velocity is very small when the particle enters the electric field. At time t = 0, $\dot{x} = 0$, therefore c_1 = -ln[a]/b. Expression (9) becomes $t = (1/b)\ln[(a - b\dot{x})/a]$. Exponentiating both sides of this expression yields $1 - e^{-bt} = (b/a)\dot{x}$ or

$$1 - e^{-bt} = (\frac{b}{a})\frac{dx}{dt} \qquad (5.10)$$

Separating variables and integrating both sides of expression (5.10) gives

$$\int (1 - e^{-bt})dt = (\frac{b}{a})\int dx$$

or

$$t + (\frac{1}{b})e^{-bt} = (\frac{b}{a})x + c_2 \qquad (5.11)$$

We evaluate the integration constant c_2 by defining the first known location of the particle as x = 0 at time t = 0. If we apply this boundary condition to equation (5.11), $c_2 = 1/b$, and

$$x = \frac{a}{b}[t + (\frac{1}{b})(e^{-bt} - 1)]$$

from which

$$a = \frac{b^2 x}{[bt + (e^{-bt} - 1)]} \qquad (5.12)$$

Re-writing equation (5.12) in terms of the definition of a and b, and solving the expression for q/m gives

$$(\frac{q}{m}) = \frac{(g/v_T)^2 x}{E[(g/v_T)t + (e^{-gt/v_T} - 1)]} \qquad (5.13)$$

This equation is the basis of our experimental technique. It evaluates charge-to-mass ratio q/m, from measurements of deflection x, over time t, and the particle's terminal velocity v_T. Electric field strength must be known, and gravitational acceleration assumed constant. Note that for large time intervals t this expression can be reduced to

$$(\frac{q}{m}) = \frac{gx}{E(v_T)t} \qquad (5.14)$$

which predicts the particle should travel with a constant x component of velocity.

The Experiment

Apparatus

Figures 7 -11 show the entire experimental apparatus. Four sub-units make up the device. The expansion chamber extracts particles from saltation, allowing some to fall into the extension tube, where they accelerate to terminal velocity. Only particles that pass through the detector enter the electric field chamber. The fourth sub-unit, the imaging system, is comprised of the detector, camera, and multi-strobes system. The purpose of this last unit is to illuminate and photograph the particles in the electric field chamber.

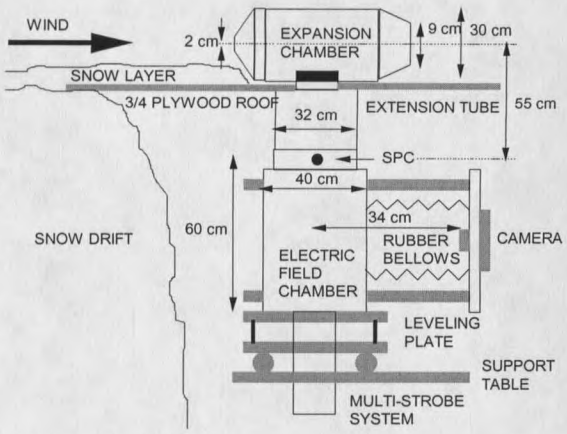

Figure 7: Apparatus for measuring charge-to-mass ratios of individual blowing snow particles

The expansion chamber (Figure 8) slows air flow and allow particles to settle. Constructed of sheet metal, the expansion chamber maintains the same ratios as the smaller drift trap reported by Mellor (1960). The expansion chamber connects to the rest of the apparatus by means of a rotating cap. This allowed the direction of the nose cone inlet to be adjusted for different wind directions. Once positioned the cap was fixed in place and sealed by an adhesive fastener (duct tape).

The extension tube (Figure 8) allows the particles to reach terminal fall velocity before entering the measurement region. Schmidt (1981) reports size distributions of saltating particles with mean equivalent diameters near 200 μm. Using standard numerical techniques to solve equations (2.16) and (2.19) assuming no lift , no electrostatic force, and approximating the drag coefficient C_d by Stoke's drag law

$$C_d = \frac{24}{Re}$$

we determined 36 cm is required for a 200 μm ice sphere to reach a terminal velocity of 125 cm s^{-1}. The vertical dimension of the extension tube was 55 cm in order to ensure that most particles attained terminal velocity. The final particle images provide a test of this requirement.

The electric field chamber is sealed, providing a still air region (Figures 9 and 10). Two aluminum plates, (Figure 9) connected to high voltage power supplies (Figure 11), produce a horizontal electric field across a 20 cm plate separation. Leveling mechanisms on the bottom

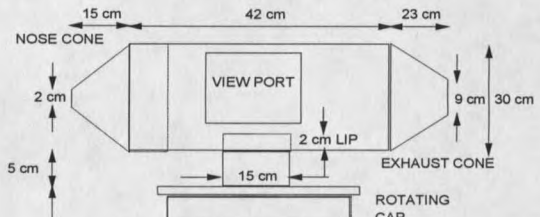

Figure 8: Expansion chamber based on Mellor's (1960) designs. Particles are extracted from saltation due to rapid expansion of air flow through the chamber. The extension tube length is designed to allow particles to reach terminal velocity before entering the electric field chamber.

corners of the chamber allow leveling to set the electric field perpendicular to gravity. Flat black paint on all interior surfaces of the chamber reduce reflections, and black velvet on the chamber wall opposite the camera gives high contrast to the particle images. The high voltage supplies, adjustable over a range of 0-20 kV, provide a variable electric field. Plate voltages measured with a high voltage probe during the experiment were +14.93 kV and -14.60 kV, giving an electric field strength E = 147.65 V mm^{-1}. Higher electric fields interfered with the particle detection circuit. The multi-strobe system (Bird and Jairell, 1989) provides continuous light from a halogen lamp, and accurately timed flashes from eight electronic strobes.

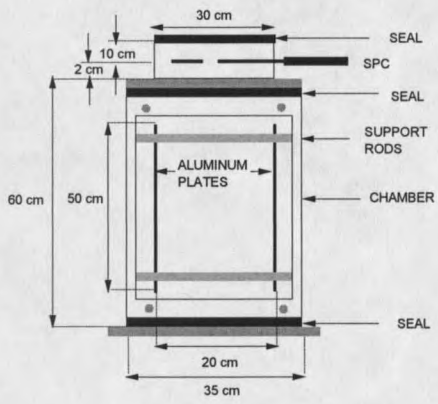

Figure 9: End view showing inside of electric field chamber. The electric field is generated by connecting high voltage supplies to the aluminum plates.

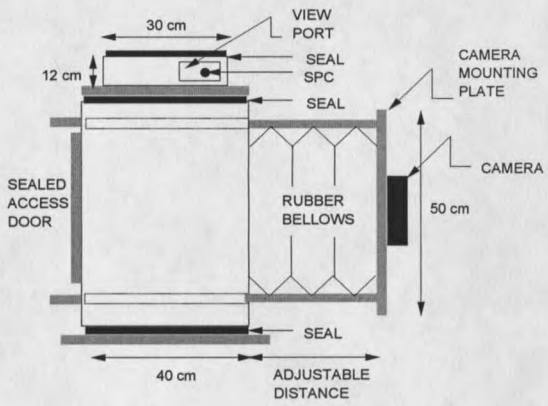

Figure 10: Side view showing outside of electric field chamber. Camera focal length is adjusted by means of a movable camera plate connected to the chamber by a rubber bellows.

The result is a photographic image showing a sequence of dots, defining particle location, along a low-intensity white streak on a black background. An adjustable slit (set to 1 cm), on a clear plastic window sealed to the bottom of the electric field chamber, confines illumination to a region perpendicular to the plane of the plates and centered in the chamber. A small fan on the multi-strobe housing removes heat produced by the halogen lamp.

The timing circuit performs two functions. It opens the camera shutter when a particle is detected, and triggers the strobe sequence after a delay that allows the particle to move from the detector into the electric field chamber. Particles are detected by a snow particle counter (SPC) that senses the particles shadow in a light beam (Schmidt, 1977).

We used a 35 mm film camera with motor drive, data back, and 55 mm, f 1.4 lens to record particle images. A microprocessor controls the timing circuit, allowing programmable time delays. For our experiment, a time delay of 121.6 ms was set between particle detection and first strobe flash, with 20.0 ms intervals between each flash.

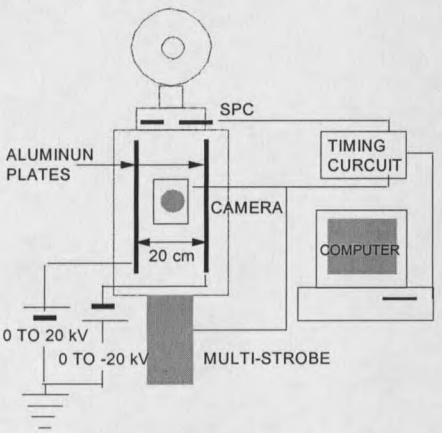

Figure 11: Schematic diagram of electric field chamber and photo-imaging system

Field Procedure

The experiment was conducted on 8 January 1996 at the Chimney Park trailhead, 96 km west of Laramie, Wyoming on Highway 130. Snowplow operators for the Wyoming Highway Department assisted us in forming a 2.1 m high snow bank, at the west end of the trail head parking lot. Suitable snow cover existed upwind of the site, though no new snow had fallen in several days. A mobile laboratory provided electricity and shelter for computers (as well as investigators). Supporting meteorological data included wind speed and direction, air temperature, and humidity, all measured 1 m above the surface near the top of the snow bank.

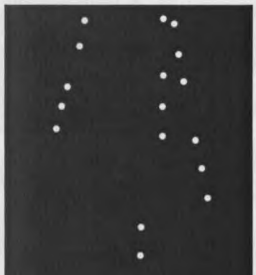

Figure 12: Image showing trajectories of the first four particles in Table 1. Strobe number five failed to flash throughout the experiment. The image was enhanced and converted to black and white for this figure.

The apparatus was set up in the parking lot just downwind of the snow bank. A roof, level with the top of the snow bank, prevented the apparatus from being drifted in (Figure 7). A 20 cm layer of snow, placed on the roof, smoothed the approach to the inlet of the device. The electric field chamber was leveled and the inlet aligned with the wind.

A length scale was defined for image analysis by suspending a metric ruler at the center of the field of view for the first two pictures of each film roll. Four rolls of 36 exposure (ASA 1600) were exposed between 1400 and 1700h, in low-level drifting (no noticeable suspension).

Analysis Procedure

Of the 136 images we exposed, 50 showed particle images. We transferred these to compact disk for analysis using computer software. Figure 12 shows an example image from which particle location was digitized. We also digitized the endpoints of the same100 mm segment in all images of the ruler, to determine a length scale.

Vertical distance between dots, divided by the 20 ms strobe interval, determined particle fall velocity. If the particle was at terminal velocity, an average value was computed for v_T. Horizontal distance between the first and last dots on the path determined horizontal deflection, x. The time, t, for this deflection was the product of the 20 ms strobe interval and the number of intervals between the first and last dot. These measured values of v_T, x, and t, together with E = 147.65 kV m^{-1}, and g = 9.81 m s^{-2} provide the arguments required to evaluate the charge-to-mass ratio of the particle using equation (5.13)

In selecting particle traces for analysis, two criteria were used to ensure particles were traveling at terminal velocity, and that measured deflections resulted only from the electrostatic force: (a) at least three strobe dots had to be visible to check for terminal velocity. (b) a trace could not approach or cross other trajectories, to be certain the deflection was not influenced by other particles.

Results

The largest variation in measured distance on the eight ruler images was less then 1%, therefore we used the average of 419 du mm^{-1} to convert coordinates of the strobe dots from digitizer units (du) to actual distance in mm. 11 traces met the criteria for analysis. Table 2 lists measurements and computed charge-to-mass ratios for these particles.

Table 2. Measurements And Computed Particle Charge-To-Mass Ratios

PARTICLE NO	v_T (mm/s)	StdDev v_T (mm/s)	x (mm)	t (ms)	q/m (μC/kg)
1	425.18	5.35	-14.53	100	-37
2	534.69	19.56	0.38	100	1
3	557.93	18.32	19.12	120	33
4	534.61	0.00	-1.15	40	-12
5	510.13	0.13	13.74	100	32
6	338.17	10.06	11.91	120	27
7	571.38	18.24	22.61	80	72
8	593.55	11.86	-11.91	120	-20
9	491.87	12.84	-26.27	100	-63
10	438.78	14.34	-18.63	40	-208
11	627.45	7.09	-10.08	40	-106

Data for the four particles in figure 12 are listed first. Wind speed decreased from 10 m s^{-1} at the beginning of sampling to 5 m s^{-1} near the end. Temperature decreased from +1°C to -2°C, with relative humidity dropping from 93% during peak drifting, to 70% as winds decreased.

Error Analysis

We estimated the errors for computed charge-to-mass ratios in Table 2 from the errors in each argument of the computation. Table 3 lists these values. A worst-case analysis for a particle with 500-mm s^{-1} fall velocity, deflected 15 mm in 100 ms by an electric field of 148 kV mm^{-1} gives a maximum error of 4% in q/m, equal to 1.5 $\mu C\ kg^{-1}$. Percent error increased as deflections decreased.

Table 3. Error Source In Particle Charge-To-Mass Computations

SOURCE OF ERROR	ERROR IN MEASUREMENT	CONTRIBUTION TO ERROR IN q/m
Time Interval (t)	$\pm$ 0.4 ms	Negligible
Deflection (x)	$\pm$ 0.6 mm	2%
Fall Velocity (v_T)	$\pm$ 15.8 mm/s	1%
Electric Field (E)	$\pm$ 1.2 V/mm	1%

Discussion

The derivation of equation (5.13) depends on two critical assumptions. (a) Particles fall at terminal velocity, and (b) the shape factor (drag coefficient) is the same in all directions. Very consistent vertical distances between dots on each trace strongly support both assumptions. Measured variations in fall velocity were random for all traces, and within the uncertainty of the measurement. We

saw no trace oscillations characteristic of particles falling with a preferred orientation (as reported for plate snow crystals, for example). The ratio of longest axis to perpendicular axis averaged 1.49 for saltating snow photographed by Schmidt (1981). Saltation impacts and non-uniform instantaneous drag on such particles will cause rotations that continue after particles enter our apparatus. These rotations should yield an average shape factor approximately constant with respect to direction.

Average charge-to-mass ratios near -10 $\mu C\ kg^{-1}$ were reported for blowing snow in the semi-arid climates of Montana (Latham and Montagne, 1970). Ratios as large as -50 $\mu C\ kg^{-1}$ were measured in Antarctica by Wishart (1970). Many particles we evaluated had charge-to-mass ratios significantly higher than average charge-to-mass ratios previously measured in semi-arid climates. The largest individual ratio was -208 $\mu C\ kg^{-1}$, four times the largest average ratio previously reported. Although knowledge of the electrification process is incomplete, we speculate that even larger ratios occur in more intense drifting.

CHAPTER SIX

CALCULATIONS OF THE ELECTROSTATIC FORCE IN SALTATION

A 120 μm particle, carrying a charge of –208 μC kg^{-1}, subject to the measured electric field of 30 μC kg^{-1}, sees an electrostatic force on the same order of magnitude as the gravitational force. In order to examine the effects of this electrostatic force on saltating snow particles trajectories, we combined the charge-to-mass ratios presented in chapter five (Schmidt et al., 1998), with the electric field measurements in chapter four (Schmidt and Dent, 1994). Ideally these measurements would be simultaneous, but the prototype instrument systems were not simultaneously available.

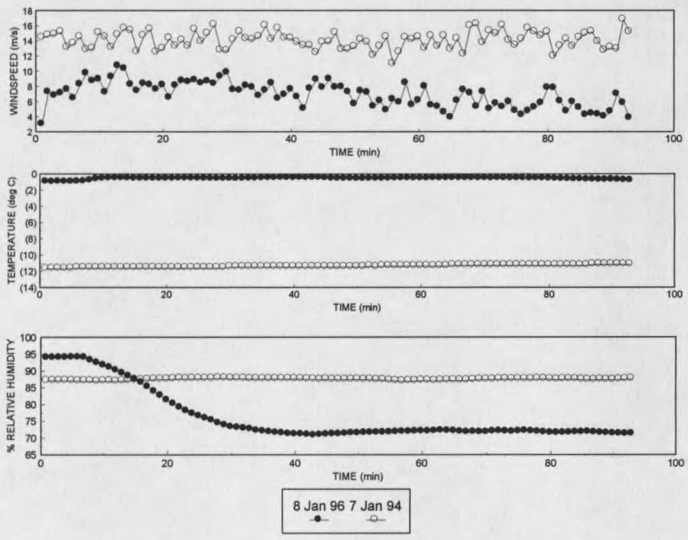

Figure 13: Comparison of wind speed, temperature, and relative humidity for the storms of 7 January 1994 and 8 January 1996.

Figure 14 shows a comparison of the meteorological data from

the storms of 7 January 1994 and 8 January 1996. Measurements were made 7 January 1994 during the night with winds averaging 14 m s^{-1} and temperatures holding steady at -12° C. Relative humidity was also a constant 87% during the period shown. The storm of 8 January 1996 was much milder with average winds of 7 m s^{-1} and temperatures only slightly below freezing. Relative humidity decreased from 94% to 70% as blowing snow transport increased. Based on the results of Latham and Stow (1967) the single most significant difference between the storms in probably the much higher wind speeds of 7 January 1994. They found charging of saltation particles to increase approximately as the square of wind speed. This would indicate that particles in transport in the 1994 storm may have carried a larger charge then those we measured in the 1996 storm. The other significant difference was temperature. Colder temperatures during the 1994 storm may also have been associated with increased charging based on the findings of Maeno et al (1985). Latham and Stow (1967) found that charging is a function of the temperature difference between the air and snow surface, however measurements of snow surface temperatures were not made during the two storms.

Trajectory Calculations

Using the electric field profile from Figure 2, we solved the equations of motion for a saltating sphere using standard numerical methods and the following assumptions:

a. particle specific gravity = 0.92, air density = 0.85 kg m^{-3}
b. initial velocity y-component = 0.8 m s^{-1}, x-component =0
c. logarithmic wind speed profile with 0.40 m s^{-1} friction velocity, threshold friction velocity = 0.35 m s^{-1}
d. particle angular velocity = 0 (no spin, to eliminate Magnus effect)
e. electric field profile E = 28 $h^{-0.6}$ (E in kV m^{-1}, h in cm, Fig. 7) particle charge = +72 μC kg^{-1} and -208 μC kg^{-1}.

The drag coefficient C_d was approximated by Carrier's drag law. Initial velocity is assumed upward and estimated by calculating the velocity required for a particle to obtain a typical saltation height of 3 cm (Kobayashi, 1972) under the influence of the gravitational force. Friction velocities, and threshold friction velocities are estimated from wind profiles measured over various snow surfaces (Tabler, 1980). The nominal particle diameter is determined by assuming the particle is a sphere. Measurements of terminal velocity from image analysis (Table 2) and the vertical equation of motion 5.4 provide particle diameter as follows. From equation 5.4

$$mg - k_y(3\pi\mu)d_n v\cos\theta = m\ddot{y} \qquad (6.1)$$

For a particle at terminal velocity v_T, $\ddot{y}$ is zero therefore

$$mg - k_y(3\pi\mu)d_n v_T\cos\theta = 0 \qquad (6.2)$$

The mass of the sphere m is

$$m = \frac{4}{3}\pi(\frac{d_n}{2})^3\rho \qquad (6.3)$$

Here, d_n is the diameter of the sphere and ρ is the density of ice. Substituting equation 6.3 into equation 6.2 and solving for d_n gives

$$d_n = [(18k_y \mu v_T) / \rho g]^{1/2} \qquad (6.4)$$

Figure 15 shows the results of the calculation for a 120 μm ice sphere with a charge of -208 μC kg^{-1}. Figure 16 shows these same calculations for a 140 μm ice sphere carrying a positive charge of 72 μC kg^{-1}. As a comparison, we

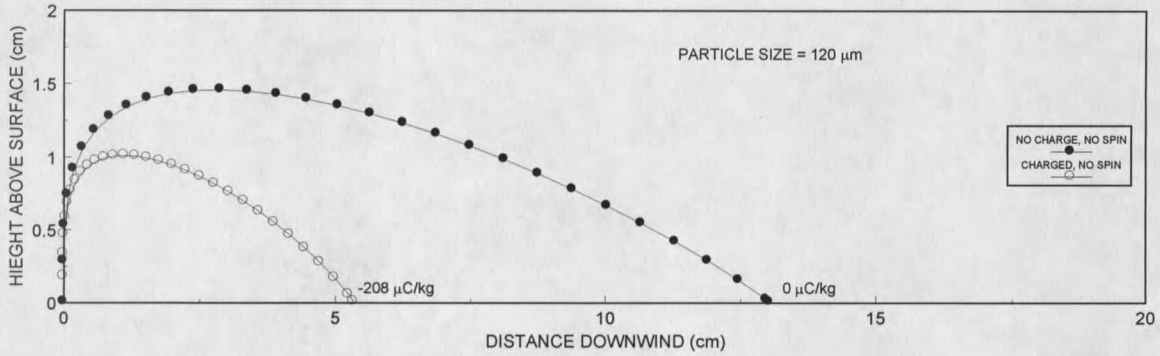

Figure 14: Saltation trajectories for 120 μm ice sphere with no charge and with a charge of -208 μC kg^{-1}. The particles saltate in the electric field defined in figure 7 and are subject to a logarithmic wind profiled with 14 m s^{-1} measured at the 1 m height.

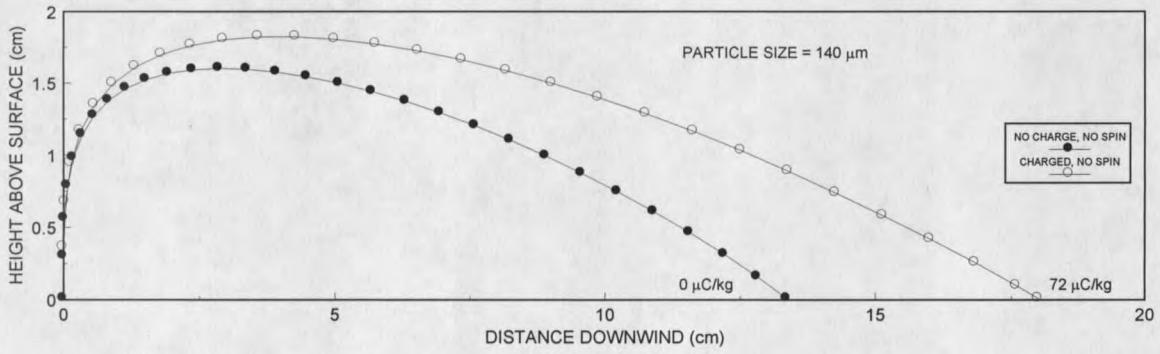

Figure 15: Saltation trajectories for 140 μm ice sphere with no charge and with a charge of 72 μC kg^{-1}. The particles saltate in the electric field defined in figure 7 and are subject to a logarithmic wind profiled with 14 m s^{-1} measured at the 1 m height.

calculated spin rates necessary to match trajectories of the 120 and 140 μm charged ice sphere (Figure 15 and 16) using Magnus lift alone. The spin rates necessary to produce trajectories comparable to those of the charged particles using Magnus lift where above 1000 rps for both particles.

Discussion

For a 120 μm particle, carrying a charge of -208 μC kg^{-1} and saltating in the measured electric field (Figure 6), the saltation trajectory is 60% shorter then that of an uncharged particle of the same size (Figure 15). Furthermore, the height of the trajectory is only 31% that of the uncharged sphere. The saltation trajectory increases 35% in length and 14% in height for the 140 μm particle carrying a positive charge of 72 μC kg^{-1} (Figure 16). Impact parameters for the saltation trajectories are also altered. The impact speed for the 140 μm particle is 145 cm s^{-1} with an impact angle of 12° with the horizontal for the charged particle. This compared to146 cm s^{-1} with an impact angle of 16° for the uncharged particle. The results are more significant for the negatively charge, 120 μm particle. Here impact velocity decreases from 125 cm s^{-1} for the uncharged particle to 116 cm s^{-1} for to charged particle with impact angles increasing from 17° to 30°. For the two charged particles of almost identical size, impact velocities differed by 20%.

These changes in trajectories and impact parameters could play a significant role in the overall saltation process and the transfer of particles

between saltation and suspended modes of transport. Impact forces from saltating particles break surface particle bonds contributing to saltation flux (Schmidt, 1981). The change in saltation trajectory height might imply that positively charged particles, rebounding higher above the surface, have a better chance of being transported in suspension compared to their negatively charged counterparts.

Measurements used to calculate the saltation trajectories in Figures 15 and 16 were made in two different storms having significantly different environmental parameters (Figure 14). A review of Latham and Stow (1967) gives some insight into comparisons of the charging mechanism for the two events but lack of needed measurements makes these comparisons mostly supposition. Consistent with (Latham and Stow, 1967) results, we observed the measured electric field to be a strong function of wind speed. Since the individual particle charge-to-mass ratios were measured at low wind speeds, we believe that calculations presented here probably under estimate the effects of electrification for many saltation particles.

Temperature and humidity must also play a role in the charging of the blowing snow particles. For the measurements made here temperature and humidity were significantly different. Experiments are needed to fully understand the role they play in particle charging.

CHAPTER SEVEN

SUMMARY AND CONCLUSION

Summary

At the onset of this investigation, the literature showed that potential gradients, much larger than the fair weather gradient develop above a surface in blowing snow. It was also known that saltating snow particles develop electrostatic charges, usually of negative sign. The primary contribution of this investigation was to show how strongly the resulting electrostatic forces can influence saltation trajectories. This was accomplished by (1) inclusion of electrostatic forces in equations describing saltation motion, (2) improved measurements of electric field in blizzard saltation, and (3) improved measurements of charge-to-mass ratio for moving particles. This section reviews these steps, and includes thoughts on how the results might be used, and implications for further research.

Calculations Of Saltation Trajectories Including The Electrostatic Force

Although charge separation in aeolian transport was recognized, electrostatic forces had apparently not been included in transport equations.

Adding the force on a charged particle moving in an electric field to the equations of motion for a saltating sphere provided the hypothesis that focused the experimental measurements. Solution of the equations, using standard numerical techniques, tested the hypothesis that the electrostatic forces significantly influenced saltation trajectories. The results showed trajectory lengths altered by as much as 60% for charged particles, compared to uncharged particles.

Electric Field Gradients In Blizzards

A model based on the physical definition of the electric field in the atmosphere and reported average particle charge-to-mass ratios (Schmidt and Dent 1993) predicted strong electric fields very near the surface in saltation. Testing this hypothesis required measurements of the electric field gradient in the region 0-10 cm above the surface, in blowing snow. The positive electric field measured in this experiment was as high as 30 kV m^{-1} at a height of 4 cm and was opposite the direction of the fair-weather field. The field gradient measured in a blowing snow storm compare well with the theoretic model developed by Schmidt and Dent (1993).

Charge-To-Mass Ratios On Blowing Snow Particles

In measuring particle charge in blowing snow by collecting a sample of wind-blown particles, the sign of the average charge sometimes switched from negative, expected from the literature review, to positive. Changes in sign correlate positively with wind gust. This observation led to the hypothesis that

positive surface particles, eroded during wind gusts, mix with negatively-charged saltation particles to reduce the average charge-to-mass ratio, determined from the charge on a sample of wind-blown snow divided by sample mass.

Using the photographic chamber, measurements on individual saltation particles showed a mixture of positive and negative particles even in low-level drifting, and confirmed the hypothesis that individual particle charge-to-mass ratios are much high than the values determined by the averaging method. Measured ratios ranged from -208 $\mu C\ kg^{-1}$ to 72 $\mu C\ kg^{-1}$, several times larger than the values previously reported.

Some Speculations About The Results

Although the results presented here were obtaind from measurements in blizzards, the modified trajectory equations should apply to other aeolian processes, such as sand and dust storms, not only in the earth's atmospheric boundary layer, but also on other planets. (Application to sand transport has already been reported by Schmidt et al. 1998).

The results also emphasize the importance of electrostatic effects when interpreting wind tunnel studies, where large electrostatic charges are observed when particles are introduced. These experiments are often confounded by particles sticking to the sides of the wind tunnel due to this electrification. This electrification may provide a mechanism that can be used to improve wind tunnel simulations of drifting. By controlling the electric field at the tunnel floor and the

charge on injected particles, saltation trajectories might be scaled, providing better simulation of drift around obstacles.

Measured electrostatic forces on saltation particles in blowing snow and sand (Schmidt, et al. 1998) are on the same order as the gravitational force at the 4 cm height. These measurements were conducted during low to moderate drifting. We speculate electrostatic forces exceed the gravitational force in the saltation region during stronger drifting events. Electrostatic and gravitational forces are conservative, so a particle acted on by these forces alone must eventually return to the ground. However, if we consider the effects of fluid drag, it becomes quite conceivable that the particles float. We expect particles subject to these forces to reach some maximum height and then proceed downwind, undergoing a dampened oscillatory vertical motion centered about the height for which the gravitational and electrostatic forces are balanced. As a test of this hypothesis we ran the numerical trajectory solutions for a 140 μm ice sphere, saltating in the electric field shown in figure 2, having charge-to-mass ratios of 300, 200, and 150 $\mu C\ kg^{-1}$. The solution was obtained using the same fluid assumptions presented in chapter six. Figure 17 shows the results for the particle with a charge-to-mass ratio of 200 $\mu C\ kg^{-1}$. The suspension transport from 60 to 100 cm occurs at the height for which gravitational and electrostatic forces are balanced. The lowest particle charge-to-mass ratio producing suspended transport in the measured electric field is approximately 150 $\mu C\ kg^{-1}$. Based on the measurements presented in Table 2, it is conceivable that some

particles carry positive charges that enable them to float. Saltation trajectory lengths for particles subject to an electrostatic force close to, but less than the gravitational force, are higher and longer, thus increasing the chance of turbulent transfer to suspended transport.

Understanding the process that transports saltation particles into suspension is critical for computer models describing aeolian processes. These models currently lack this information. The results presented suggest electrostatic forces are important in this process. In order to assess the effects of electrification on suspended transport, experiments measuring charge distribution through and above the saltation layer are needed. These

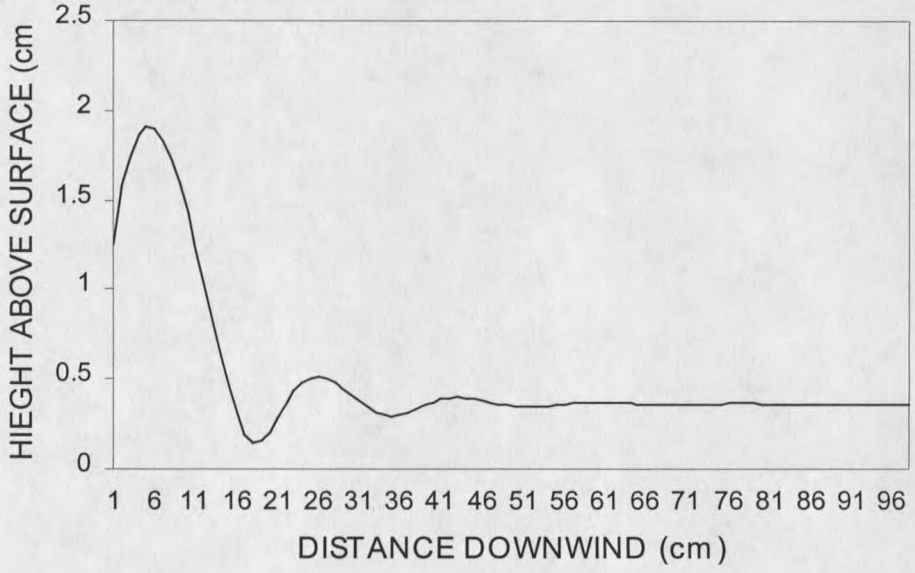

Figure 16: Saltation trajectory for a 140 μm ice sphere with a charge-to-mass ratio of 200 μC kg^{-1}. The particle saltates in the electric field defined in figure 2 and is subject to a logarithmic wind profile with 14 m s^{-1} measured at the 1 m height. The equalibrium suspension height matches the height at which the gravitational and elecrostatic forces are equal.

experiments should also relate charge distribution to saltation particle size.

Latham and Montagne (1970) explored the role electrostatics might play in formation of snow cornices. They recommended "considerable further study," which seems warranted in view of results presented here. The electric fields measured here were over relatively flat surfaces. The pointed shape at the leading edge of the cornice will significantly enhance this electric field so that negatively charged particles, moving over a positive cornice surface, see a substantial attractive force. This may be the mechanism that allows the particle to be held on the lip of the cornice long enough for sintering to take place.

Electrostatics may explain roadway icing during blizzards. If a road surface becomes positive or negatively charged due to asymmetric rubbing, charged particles of opposite sign may stop on the surface. Resulting snow patches would be converted to ice patches under compaction by passing vehicles. If this is true, icing of road surfaces might be prevented by reducing surface charge development or by steering the particles with an additional electric field.

Understanding of aeolian electrification might be enhanced by investigation of surface charge on drift formations. Consider a surface of newly fallen snow. At the onset of transport predominately negatively charged particles saltate over a surface of positive charge. Deposition behind terrain features due to disruption of airflow should result in areas of negative surface charge. Positively charged surface particles eroding up-wind of the deposition area create a charge separation and development of a negative electric field.

Saltation trajectories decay for positively charged particles with an increase in trajectory lengths for particles carrying a negative charge. The likelihood of positive particles depositing on the surface, combined with the thermoelectric effect, should eventually lead to the return of a positive surface and positive electric field. The existence of areas of positive and negative charge, and the association of these zones of erosion and deposition would provide strong evidence supporting of refuting our current understanding of the charging process. This may very well be the next critical experiment needed to extend our understanding of aeolian electrification.

Nature tends to a balance, suggesting self-regulation of electrification exists. The idea of self-regulation in saltation is not a new one. Owen (1964) suggests that a negative feed back exists in saltation. Particles in saltation present a substantial drag on the wind thereby extracting energy from the vertical velocity profile. He argues this has the effect of maintaining the surface shear stress at the level associated with the threshold wind speed. Owen's negative feed back hypothesis may imply a limiting factor on saltation electrification since it appears to be a strong function of wind speed and dependent on transport rate. There may be some separate self-regulating process for electrification. Particles experiencing an attractive electrostatic force do not rebound as high and therefore remove less energy from the vertical velocity profile. This allows higher wind speeds, increasing the electric field. The increased attractive force decays saltation which in turn reduces electrification, allowing particles to obtain the higher saltation trajectories needed to enhance saltation. This same line of

reasoning leads to a balance on electrification due to positive particle transport. This balance may help to explain differences between theoretical and measured transport rates.

Conclusion

The electrostatic force on a saltating snow particle can be as large as the gravitational force and has a significant effect on saltation trajectories. Through charge separation, a strong electric field develops within the saltation region. The field is usually positive, indicating negatively charged particles above a surface of positive charge, but moving particles with positive charge were also found. Magnitudes of both field and particle charge-to-mass ratios were larger than previously reported, changing calculated trajectory lengths by as much as 60 percent. The strength of electrostatic forces may help explain the rate at which particles move from saltation to suspended transport mode.

REFERENCES CITED

Barré, M. 1953. Propriété électriques du blizzard. Ann. Geoph. 9 (2), 164-166.

Bagnold, R.A. 1941. The Physics of Blowing Sand and Desert Dunes. Methuen, London.

Bird, K.G. and Jairell, R.L. 1989. Sequential Flash for Photographing Trajectories of Saltating Snow Particles. Proc. 57th Western Snow Comference, Apr 18-20, 1989, Fort Collins. CO., USA, pp. 130-133.

Camp, P.R. 1976. Charge, Morphology, and pH of Natural Snow. J. Geophys. Res., 81(9), 1589-1592.

Gilbert, G. K. 1914. Transportation of debris by running water. United States Geological Survey Professional Paper 86. U.S. Government Printing Office, Washington, DC. pp. 267.

Gross, G. W. 1982. Role of relaxation and contact times in charge separation during collision of precipitation particles with ice targets. J. Geophys. Res., Vol. 87, No. c9, pp 7170-7178.

Henry, P.S.H. 1953. The role of asymmetric rubbing in the generation of static electricity. Brit. J. Appl. Phy., Supp., 2, S31-S36.

Hobbs, P.V. 1974, Ice Physics. Oxford. Clarendon Press.

Iribarne, J. V., and H. R. Cho, Atmospheric Physics, Reidel Publishing Co., Dordrecht, Holland, 1980.

Johnston, A.R. and Kirkham, H. 1989. A Miniaturized Space-Potential DC Electric Field Meter. IEEE Trans Power Deliv., 4(2), 1253-1261.

Kikuchi, T. 1981. A wind tunnel study of the aerodynamic roughness associated with drifting snow. Cold Reg. Sci. Technol., 5, 107-118.

Kobayashi, D. 1972. Studies of snow transport in low-level drifting snow. Contrib. Inst. Low. Temp. Sci. Hokkaido Univ., Ser. A(24), 1-58.

Latham, J. 1963 Electrification produced by the asymmetric rubbing of ice on ice. Brit. J. App. Phys.,14(8), 488-490.

Latham, J. and Mason , B. J. 1961. Electric charge transfer associated with temperature gradients in ice. Proc. R. Soc., Ser. A, 260(1303), 523-536.

Latham, J. and Miller, A.H. 1965. The role of specimen geometry and impact velocity in the Reynolds-Brook theory of thunderstorm electrification. J. Atmos. Sci., 22, 505-508.

Latham, J. and Montagne, J. 1970. The possible importance of electrical forces in the development of cornices. J. Glaciol., 9(57), 375-384.

Latham, J. and Stow, C.D. 1965. Electrification produced by collision between ice crystals and soft hail pellets in a thunderstorm. Quart. J. R. Met. Soc., 91, 99-100.

Latham, J. and Stow, C. D. 1967. A laboratory investigation of the electrification of snowstorms. Quart. J. R. Met. Soc., 93, 55-68.

Maeno, N., Araoka, K., Nishimura, K., and Kaneda, Y. 1979 Physical aspects of the wind-snow interaction in blowing snow. J. Fac. Sci., Hokkaido Univ., Ser. VII 6(1), 127-141.

Maeno, N., Naruse, R., Nishimura, K., Takei, I., Ebinuma, T., Kobayashi, S., Nishimura, H., Kaneda, Y., and Ishida, T., 1985. Wind-tunnel experiments on blowing snow. Annals of Glaciology 6, 63-67.

Magono, C. and Sakurai, K. 1963. On the electric charge of drifting snow pellets. J. Met. Soc. Japan, 41, 211-217.

McNown, J.S., Malaika, J., and Pramanik, R. 1951. Particle Shape and Settling Velocity. Trans. 4th Meeting of the International Association for Hydraulic Research, Bombay India, 1951, pp. 511-522.

Mellor, M. 1960. Gauging Antarctic Drift Snow. Antarctic Meteorology, Pergamon Press, New York, pp. 347-359.

Millikan, R.A. 1910. Electrons, Protons, Photons, Neutrons, Mesotrons, and Cosmic Rays, 2ND edition. University of Chicago Press, Chicago, 1947.

Owen, P. R. 1964. Saltation of uniform grains in air, J. Fluid Mech., 20, pp. 225-242.

Pearce, P. C. and Currie, B. W. 1949. Some qualitative results on the electrification of snow. Canad. J. Res., 27A(1), 1-8.

Reynolds, S.E., Brook, M. and Gourley, M.F. 1957. Thunderstorm charge separation. J. Met., 14, 426-436.

Schaefer, V. J. 1947. Properties of particles of snow and the electrical effects they produce in storms. Trans. Amer. Geophys. Un., 28(4), 587-592.

Schmidt, R. A., 1977. A system that measures blowing snow. USDA Forest Service Research Paper RM-194, 80 p.

Schmidt, R.A. 1980. Threshold wind-speeds and elastic impact in snow transport. J. Glaciol., 26(94), 453-467.

Schmidt, R.A. 1981. Estimates of threshold windspeed from particle sizes in blowing snow. Cold Reg. Sci. and Technol., 4, 187-193.

Schmidt, R. A. 1982. Properties of blowing snow. Reviews Geophys. and Space Phys., 20(1), 39-44.

Schmidt, S. and Schmidt R.A. 1992. The Sign Of Electrostatic Charge On Drifting Snow. Proc. International Snow Science Workshop, Oct 4-8, 1992, Breckenridge, CO, USA. pp. 351 -360.

Schmidt, S. and Dent, J.D. 1993. A Theoretical Prediction of the Effects of Electrostatic Forces On Saltating Snow Particles. Ann. Glaciol., 18, pp. 234-238.

Schmidt, S. and Dent, J.D. 1994. Measurements Of The Electric Field Gradient In a Blizzard. Proc. International Snow Science Workshop, Oct. 30-Nov.3, 1994, Snowbird, UT, USA. pp. 197-202.

Schmidt, D.S., Dent J. D., and Schmidt R. A. 1998. Charge-to-mass ratios of individual blowing snow particles, Annals Glaciol., 26, pp. 207-211.

Schmidt, D.S., Schmidt, R.S., and Dent, J.D. Electrostatic Force On Saltating Sand. J. Geophys. Res., Vol. 103, No. D8, pp 8997-9001.

Schonland, B. F. J., Atmospheric Electricity, Methuen and Co. LTD., London, 1953.

Scott, W.D. and Hobbs, P.V. 1968. The spectra of charging events due to the collision of natural ice particles with an ice surface. Quart. J. R. Met. Soc., 94, 510-533.

Scott, W.D. and Hobbs, P.V. 1968. The spectra of charging events due to the collision of natural ice particles with an ice surface. Quart. J. R. Met. Soc., 94, 510-533.

Scott, W.D. and Levin, Z. 1970. The effects of a potential gradient on the charge separation during interaction of snow crystals with ice spheres. J. Atmos. Sci., 27, 463-473.

Sheppard, P. A. 1937. British Polar Year Expedition, Fort Rae, 1932-1933, discussion of results, Vol. 1:Atmospheric electricity. Roy. Soc., London, p.319.

Simpson, G. C. 1921. British Antarctic Expedition, 1910-1913. Vol. 1, London, Harrison and Sons.

Tabler, R. D., 1980. Self-similarity of wind profiles in blowing snow allows outdoor modeling. J. Glaciology 26(94):421-433.

Tabor, D. 1951. The Hardness of Metals. Clarendon Press, Oxford, pp. 175.

White, B. R., Particle trajectories of saltating grains in terrestrial and Martian atmospheres, Ph.D. dissertation, Iowa State Univ., Ames, 1975.

White, B. and Schultz, J. 1977. Magnus effects in saltation. J. Fluid Mech., 81, part 3, 495-512.

Wishart, E. R. 1970. Electrification of Antarctic drifting snow. Proc. Int. Symposium Antarctic Glaciological Exploration, Sept. 3-7, 1968, Hanover, NH, USA. IASH Pub. No. 86, 1970, p. 316-324.

Wishart, E. R. and Radok, U. 1967. Electrostatic charging of aerial wires during Antarctic blizzards. Polar Meteorology, Techn. Note, No. 87, WMO-No. 211.TP.111, p. 492-529.

Workman, E. J. and Reynolds, S. E. 1950. Electrical phenomena occurring during the freezing of dilute aqueous solutions and their possible relationship to thunderstorm electricity, Phys. Rev., 78, p. 254-259.